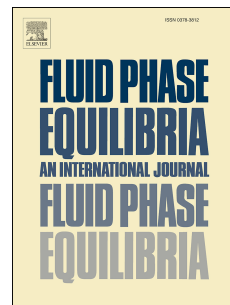


Journal Pre-proof

Thermodynamic modeling of CO₂ absorption in aqueous potassium carbonate solution with electrolyte NRTL model

Harnoor Kaur, Chau-Chyun Chen



PII: S0378-3812(19)30400-5

DOI: <https://doi.org/10.1016/j.fluid.2019.112339>

Reference: FLUID 112339

To appear in: *Fluid Phase Equilibria*

Received Date: 26 July 2019

Revised Date: 21 September 2019

Accepted Date: 30 September 2019

Please cite this article as: H. Kaur, C.-C. Chen, Thermodynamic modeling of CO₂ absorption in aqueous potassium carbonate solution with electrolyte NRTL model, *Fluid Phase Equilibria* (2019), doi: <https://doi.org/10.1016/j.fluid.2019.112339>.

This is a PDF file of an article that has undergone enhancements after acceptance, such as the addition of a cover page and metadata, and formatting for readability, but it is not yet the definitive version of record. This version will undergo additional copyediting, typesetting and review before it is published in its final form, but we are providing this version to give early visibility of the article. Please note that, during the production process, errors may be discovered which could affect the content, and all legal disclaimers that apply to the journal pertain.

© 2019 Published by Elsevier B.V.

Thermodynamic Modeling of CO₂ Absorption in Aqueous Potassium Carbonate Solution with Electrolyte NRTL Model

Harnoor Kaur, Chau-Chyun Chen*

Department of Chemical Engineering, Texas Tech University, Lubbock, TX 79409-3121, USA

* Corresponding author. Tel.: +1 806.834.3098. Email address: chauchyun.chen@ttu.edu

ORCID: Chau-Chyun Chen: 0000-0003-0026-9176

Abstract

Aqueous potassium carbonate (K₂CO₃) solution is a favorable choice for CO₂ removal due to low costs and lessened environmental impacts compared to amine solutions. To support process development of CO₂ removal with aqueous solutions, we present a comprehensive thermodynamic model for the H₂O + K₂CO₃ + CO₂ ternary system using electrolyte Nonrandom Two-liquid (eNRTL) activity coefficient model. Experimental data of vapor-liquid equilibrium, heat capacity, excess enthalpy, mean ionic activity coefficient and osmotic coefficient are simultaneously used to determine the temperature dependent eNRTL binary interaction parameters for the ternary system and its binary subsystems. Covering a wide temperature range of 273.15 to 473.15 K, the K₂CO₃ concentration up to saturation, and the CO₂ loading range of 0 to 3.6, the model satisfactorily represents all the thermodynamic properties for the system. The model should be a very useful tool in the research, development and design of CO₂ capture processes involving concentrated K₂CO₃ solutions at elevated temperatures and pressures.

Keywords:

CO₂ absorption; electrolyte NRTL model; potassium carbonate solution; solid-liquid equilibrium; vapor-liquid equilibrium

1. Introduction

Carbon dioxide is the major contributor to global warming. Tremendous efforts on CO₂ capture have been pursued globally to reduce its emissions from industrial facilities such as coal-fired power plants, steel and cement plants, and petrochemical complexes. Among the various CO₂ capture technologies available today, chemical absorption remains the most feasible option.

Monoethanolamine, monodiethanolamine and various other alkanolamines have been the leading chemical absorbents for CO₂ capture for decades. Although they are effective in removing CO₂ at typical flue gas conditions in coal-fired power plants, they are not suitable solvents for CO₂ absorption at elevated temperatures and pressures [1-3]. Alkanolamines are hazardous, have significant volatility, and are chemically unstable in the presence of oxygen. In addition, alkanolamines are highly corrosive and viscous, and they must be diluted in water for industrial use. All these issues result in high solvent loss albeit with extra equipment and high energy requirement for solvent regeneration. [2, 4-6].

Known as the “Benfield Process,” scrubbing of CO₂ by potassium carbonate solutions is commercially beneficial when operating at elevated temperatures and pressures. The concentration of hot, concentrated aqueous K₂CO₃ solution employed in the Benfield process is approximately 20 to 40 wt.% whereas the CO₂ loading (moles of CO₂/moles of K₂CO₃) is roughly in the range of 0.2 to 0.7 [1, 5]. Typically the gas absorption occurs at elevated temperatures above 343 K and elevated pressures higher than 2 MPa, whereas gas desorption takes place at high temperatures of about 403 K [1, 7, 8]. Given that the absorption takes place at close to the desorption temperature, the energy required for the regeneration of the scrubbing agent is reduced and the heat exchange equipment may be eliminated. Furthermore, the loss of

scrubbing agent is of no concern because potassium carbonate has negligible volatility, slow degradation, and high CO₂ absorption capacity and stability. [1, 5, 9]

Concentrated K₂CO₃ solutions suffer from a few drawbacks for CO₂ capture at low temperatures and pressures. Application of this technology in the power generation sector is hampered by the slow reaction kinetics of CO₂ absorption with potassium carbonate solutions at prevailing low temperatures (318 to 338 K). Addition of promoters or other additives is practiced to increase the rate of reaction [2, 5]. Some of these promoters are primary and secondary amines such as diethanolamine which is the original Benfield promoter, piperazine [10], inorganic acids and amino acids [11, 12].

Many thermodynamic modeling studies have been reported for the H₂O + K₂CO₃ + CO₂ ternary system to support process development efforts involving the Benfield process. Chen et al. [13] reformulated and extended the Pitzer equation [14, 15] to develop a rigorous thermodynamic model for the ternary in the temperature range of 343.15 K to 413.15 K and the equivalent K₂CO₃ concentration up to 40 wt.%. The model results showed a satisfactory agreement with the experimental equilibrium vapor pressure data. Later, Kamps et al. [7] reported a vapor-liquid equilibrium model of the ternary based on the Pitzer equation. The model covered a temperature range of 313.15 to 413.15 K, the CO₂ loading in the range of 0.7 to 3.6, the pressures in the range of 0.27 to 9.2 MPa and the K₂CO₃ molality in the range of 0.43 to 1.7 molal. Recently, Bohloul et al. [16] presented their Pitzer model results at temperatures of 313.15, 323.15 and 333.15 K, the K₂CO₃ solution concentrations of 15, 20 and 30 wt.%, the pressure up to 1.2 MPa, and the CO₂ loading in the range of 0.4 to 1.25.

Cullinane and Rochelle [17] modeled the CO₂ solubility in aqueous solutions of piperazine and K₂CO₃ using the eNRTL activity coefficient model [18] in 0.6-2.6 molal

piperazine, 2.5-6.2 molal K_2CO_3 at 313.15 to 383.15 K, and the CO_2 loading in the range of 0.3 to 0.7. Later Hilliard [19] modeled the $\text{H}_2\text{O} + \text{K}_2\text{CO}_3 + \text{CO}_2$ ternary using the eNRTL model. His work covered a temperature range of 313.15 to 403.15 K, the CO_2 loading of 0 to 1, and the K_2CO_3 concentrations of 20 wt.%, 30 wt.% and 40 wt.%. Extending the work of Hilliard [19] and Cullinane and Rochelle [17], Endo et al. [4] described the vapor-liquid equilibrium of the ternary with 30 wt.% K_2CO_3 solution plus 0, 3 and 5 wt.% boric acid at 323.15 and 343.15 K and the CO_2 loading of 0.15 to 0.4. Also using the eNRTL model, Lee et al. [3] investigated the CO_2 partial pressure and salt solubility in aqueous K_2CO_3 solutions by adding different concentrations of glycine as a promoter. Their model covered a temperature range of 278.15 to 403.15 K, the CO_2 loading of 0 to 1, and the K_2CO_3 concentration in the range of 20 to 50 wt.%.

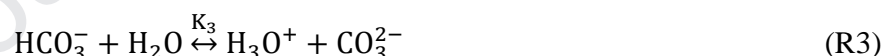
Despite the numerous thermodynamic modeling efforts for the Benfield process, these prior models are all limited in scope in terms of temperature range, K_2CO_3 concentration, and CO_2 loading. Moreover, they do not cover all the thermodynamic properties such as salt solubilities and calorimetric properties such as enthalpy that are critical when simulating and designing industrial processes. Therefore, this work aims at developing a comprehensive thermodynamic model in support of process simulation and design of the Benfield process. The eNRTL activity coefficient model has been previously applied successfully for developing comprehensive thermodynamic models for CO_2 absorption in aqueous solutions of ammonia and various alkanolamines [20-23]. To expand on this extensive library of thermodynamic models for CO_2 absorption with chemical absorbents, we use the eNRTL activity coefficient model to accurately represent all thermodynamic properties including vapor-liquid equilibrium (VLE) and solid-liquid equilibrium of the $\text{H}_2\text{O} + \text{K}_2\text{CO}_3 + \text{CO}_2$ ternary and its binary subsystems. The vapor phase properties are calculated with the PC-SAFT equation-of-state [24]. The model is valid with

the temperature range of 273.15 to 473.15 K, the K_2CO_3 concentration up to saturation, and the CO_2 loading range of 0 to 3.6.

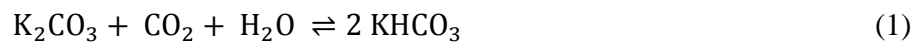
2. Thermodynamic Framework

2.1 Chemical Reactions

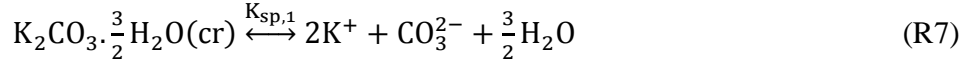
Figure 1 shows a schematic representation of all the molecular and ionic species considered for the $\text{H}_2\text{O} + \text{K}_2\text{CO}_3 + \text{CO}_2$ ternary system. The vapor phase contains molecular species CO_2 and H_2O . In the liquid phase, H_2O exists in equilibrium with its ionic species H_3O^+ and OH^- , whereas CO_2 dissociates to form bicarbonate (HCO_3^-) and carbonate (CO_3^{2-}) ions. Before reaching the saturation limits, electrolyte K_2CO_3 and electrolyte KHCO_3 represent the ion pairs of K^+ and CO_3^{2-} ions and K^+ and HCO_3^- ions, respectively. Chemical reactions involved in the solution are expressed as follows:



The ionic species H_3O^+ and OH^- are in trace amount. Therefore, the solution nonideality is dominated by the molecule-molecule, molecule-ion, and ion-ion interactions among the dominant molecular species CO_2 and H_2O and ionic species K^+ , CO_3^{2-} and HCO_3^- . The overall reaction that occurs during the absorption of CO_2 by an aqueous solution of K_2CO_3 is:



Above their saturation limits, electrolyte K_2CO_3 and electrolyte KHCO_3 precipitate as a hydrated potassium carbonate salt ($\text{K}_2\text{CO}_3 \cdot \frac{3}{2}\text{H}_2\text{O}$) and an anhydrous KHCO_3 salt, respectively [25, 26]. These salt precipitation reactions can be expressed as follows:



2.2 Vapor-Liquid Equilibrium

The equality of fugacity in the liquid and vapor phases for each component is the equilibrium criterion considered in VLE.

$$P y_i \varphi_i = x_i \gamma_i f_i^\circ \quad (2)$$

where P is the system pressure, y_i is the vapor phase mole fraction of component i , φ_i is the vapor phase fugacity coefficient calculated using PC-SAFT EoS [24], x_i is the liquid phase mole fraction, γ_i is the liquid phase activity coefficient, and f_i° is the liquid fugacity at the system temperature and pressure. The PC-SAFT EoS parameters for CO_2 and H_2O are enlisted in Table 1. Henry's law can be used to express the liquid fugacity of CO_2 in the aqueous solution; details of these expressions are readily available in the literature [20, 21, 27].

Liquid phase activity coefficient, γ_i , is calculated with the symmetric eNRTL activity coefficient model [28]. The thermodynamic framework of this model has been extensively described in the literature [29]. Briefly, the model assumes that the excess Gibbs free energy, G^{ex} , is the sum of two terms: (i) the local composition term accounting for the short-range interactions between ions and molecules, $G^{ex,lc}$, and (ii) the Pitzer-Debye-Hückel term accounting for the long-range electrostatic interaction term, $G^{ex,PDH}$.

$$G^{ex} = G^{ex,lc} + G^{ex,PDH} \quad (3)$$

For each species, the activity coefficient, γ_i is expressed in terms of G^{ex} as:

$$\ln\gamma_i = \frac{1}{RT} \left(\frac{\partial G^{ex}}{\partial n_i} \right)_{T,P,n_j \neq i} \quad (4)$$

Water activity, a_w , osmotic coefficient, ϕ , mole fraction-scale mean ionic activity coefficient, γ_{\pm}^* , and molality-scale mean ionic activity coefficient, $\gamma_{\pm m}^*$, can be calculated from the activity coefficients of various species [29]. The expressions for liquid molar enthalpy, excess enthalpy, and heat capacity have been given in the literature [27, 29]. Table 2 enlists the thermodynamic constants for H₂O and ionic species at the standard state of 298.15 K and 0.1 MPa.

2.4 Solid-Liquid Equilibrium

The solubility product constant, K_{sp} , for describing solid-liquid equilibrium of salt precipitation reactions can be expressed as follows.

$$\ln K_{sp}(T) = -\frac{\Delta G_k^o(T_{ref})}{RT_{ref}} + \frac{\Delta H_k^o(T_{ref})}{R} \left(\frac{1}{T_{ref}} - \frac{1}{T} \right) + \frac{\Delta C_{p,k}^o(T_{ref})}{R} \left[\frac{T_{ref}-T}{T} + \ln \frac{T}{T_{ref}} \right] \quad (5)$$

where ΔG_k^o is the change in Gibbs free energy, ΔH_k^o is the change in enthalpy, and $\Delta C_{p,k}^o$ is the change in heat capacity when the solid crystal k dissolves into its constituent ionic species and water molecules at reference temperature, T_{ref} of 298.15 K. Table 3 compares the values of the thermodynamic constants available in the literature with the values regressed in this work using salt solubility data.

Table 4 presents a summary of all the pure component and binary interaction parameters either available in the literature or regressed in this work.

3. Experimental Data and Regression

Substantial amount of data is available in the literature for the $\text{H}_2\text{O} + \text{K}_2\text{CO}_3$ binary, the $\text{H}_2\text{O} + \text{KHCO}_3$ binary, and the $\text{H}_2\text{O} + \text{K}_2\text{CO}_3 + \text{CO}_2$ ternary systems. Used to quantify the various model parameters, these data are summarized in Table 5 along with the mean relative deviations (MRD's) of model correlation results with experimental data. Note that the $\text{H}_2\text{O} + \text{KHCO}_3$ binary is included because CO_2 absorption in aqueous K_2CO_3 solution leads to the formation of KHCO_3 .

3.1 Experimental data for $\text{H}_2\text{O} + \text{K}_2\text{CO}_3$ binary system

Aseyev [30] reported smoothed data for the H_2O vapor pressure at aqueous K_2CO_3 concentrations in the range of 2 to 76 wt.% and temperature varying from 298.15 to 623.15 K. They also reported smoothed heat capacity data for aqueous K_2CO_3 solution in the range of 2 to 50 wt.% and temperature varying from 283.15 to 463.15 K. Roy et al. [31] and Sarbar et al. [32] reported data for the osmotic coefficient and molality-scale mean ionic activity coefficient at 298.15 K and K_2CO_3 concentration from 0.001 to 8 molal. The enthalpy of formation data was reported by Wagman et al. [33] at 298.15 K and 0.1 MPa with molar ratios of H_2O to K_2CO_3 in the range of 10 to 10,000. For the purpose of regression, these data are converted into excess enthalpy data.

3.2 Experimental data for $\text{H}_2\text{O} + \text{KHCO}_3$ binary system

Aseyev [30] reported smoothed data for H_2O vapor pressure in aqueous KHCO_3 solution at 298.15 K and KHCO_3 concentration in the range of 2 to 20 wt.%. They further reported smoothed heat capacity data for aqueous KHCO_3 solution with KHCO_3 concentration ranging from 4 to 22 wt.% in the temperature range of 278.15 to 473.15 K. Roy et al. [31] presented the osmotic coefficient and molality-scale mean ionic activity coefficient data at 298.15 K with KHCO_3 concentration in the range of 0.001 to 2 molal.

3.3 Experimental data for $H_2O + K_2CO_3 + CO_2$ ternary system

Extensive VLE data for the $H_2O + K_2CO_3 + CO_2$ ternary system are available at varying temperature, pressure, K_2CO_3 concentration, and CO_2 loading. Tosh et al. [8] reported equilibrium CO_2 partial pressure over aqueous solutions of 20 wt.%, 30 wt.% and 40 wt.% K_2CO_3 at the CO_2 loading in the range of 0 to 1.0 and a temperature range from 343.15 to 413.15 K. Korbutova et al. [34] reported CO_2 partial pressure over 20 wt.%, 25 wt.% and 30 wt.% aqueous K_2CO_3 solutions at temperatures in the range of 313.15 to 353.15 K with the CO_2 loadings varying from 0.1 to 0.42. Park et al. [9] reported CO_2 partial pressure over 5 wt.% and 10 wt.% aqueous K_2CO_3 solutions at 298.2 and 323.2 K and the CO_2 loading range of 0.7 to 1.8. Pérez-Salado Kamps et al. [7] presented total system pressure over 0.43 to 1.7 molal aqueous K_2CO_3 solutions in the temperature range of 313.15 to 393.15 K and the CO_2 loading range of 0.7 to 3.6. Endo et al. [4] reported CO_2 partial pressure over a 30 wt.% K_2CO_3 solution at 323.15 and 343.15 K and low CO_2 loadings in the range of 0.15 to 0.40. Jo et al. [35] reported CO_2 partial pressure over a 30 wt.% K_2CO_3 solution at temperatures of 373.15 and 393.15 K and the CO_2 loading varying from 0.1 to 1.0. Recently, Bohloul et al. [16] reported total system pressure over 15 wt.%, 20 wt.% and 30 wt.% aqueous K_2CO_3 solutions at 313.15, 323.15 and 333.15 K and CO_2 loadings varying from 0.4 to 1.25.

3.4 Experimental data for precipitating solids

At saturation, K_2CO_3 precipitates out as a hydrated K_2CO_3 crystal ($K_2CO_3 \cdot \frac{3}{2}H_2O$). Seidell [25] reported the solubility of K_2CO_3 in H_2O at temperatures from 273.15 to 403.15 K at the saturated vapor pressures of the solution, whereas Moore et al. [26] reported the solubility at temperatures from 384.15 to 529.15 K. On the other hand, $KHCO_3$ precipitates out to form an

anhydrous KHCO_3 crystal at saturation. Seidell [25] reported the solubility of KHCO_3 in H_2O at temperatures from 273.15 to 343.15 K at the saturated vapor pressures of the solution.

3.5 Data Regression

Regression and data analysis has been performed using Aspen V8.8 [36]. Given the dominant molecular species CO_2 and H_2O and ionic species K^+ , CO_3^{2-} and HCO_3^- , the eNRTL binary interaction parameters required for representing the Benfield process are associated with the molecule-electrolyte pairs of $\text{H}_2\text{O}-(\text{K}^+, \text{CO}_3^{2-})$, $\text{H}_2\text{O}-(\text{K}^+, \text{HCO}_3^-)$, $\text{CO}_2-(\text{K}^+, \text{CO}_3^{2-})$ and $\text{CO}_2-(\text{K}^+, \text{HCO}_3^-)$ and the electrolyte-electrolyte pair of $(\text{K}^+, \text{CO}_3^{2-})-(\text{K}^+, \text{HCO}_3^-)$. The remaining binary interaction parameters are set to their default values in Aspen Plus databank [36]. The binary interaction parameters associated with the dominant species and the solubility product constants are identified by carrying out three regression cases:

Case I-This case quantifies the temperature dependent binary interaction parameters for the $\text{H}_2\text{O}-(\text{K}^+, \text{CO}_3^{2-})$ pair by regressing the data on vapor pressure [30], heat capacity [30], mean ionic activity coefficient and osmotic coefficient [31, 32] and liquid molar enthalpy [33] for the $\text{H}_2\text{O} + \text{K}_2\text{CO}_3$ binary system. The vapor pressure data in the temperature range of 298.15 to 473.15 K are used in the regression. The heat capacity data at moderate temperatures of 283.15 to 373.15 K are used for regression purposes, whereas the data at higher temperatures are used only for comparison purposes. This is because the quality of the smoothed heat capacity data of Aseyev [30] is unknown.

Case II- With the temperature dependent binary interaction parameters for the $\text{H}_2\text{O}-(\text{K}^+, \text{CO}_3^{2-})$ pair identified in *Case I*, *Case II* further identifies the temperature dependent binary interaction parameters of the $\text{H}_2\text{O}-(\text{K}^+, \text{HCO}_3^-)$ pair, the $\text{CO}_2-(\text{K}^+, \text{HCO}_3^-)$ pair, the $\text{CO}_2-(\text{K}^+, \text{CO}_3^{2-})$ pair and the $(\text{K}^+, \text{CO}_3^{2-})-(\text{K}^+, \text{HCO}_3^-)$ pair simultaneously. The data regressed in *Case II* include the

vapor pressure [30], heat capacity [30], mean ionic activity coefficient and osmotic coefficient [31] data of the $\text{H}_2\text{O} + \text{KHCO}_3$ binary system and the VLE [4, 7-9, 34, 35] data of the $\text{H}_2\text{O} + \text{K}_2\text{CO}_3 + \text{CO}_2$ ternary system. Following the treatment in *Case I*, the heat capacity data of Aseyev [30] at moderate temperatures of 278.15 to 378.15 K are used in the regression, whereas the data at high temperatures are only used for comparison.

Case III- After all the binary interaction parameters are identified, *Case III* identifies the thermodynamic constants for precipitating salts of K_2CO_3 and KHCO_3 by regressing the salt solubility data of Seidell et al. [25] and Moore et al. [26].

The standard deviations assigned to the experimental data in the three regression cases are as follows:

- error free for temperatures of all available experimental data.
- 10% for H_2O vapor pressure in $\text{H}_2\text{O} + \text{K}_2\text{CO}_3$ and $\text{H}_2\text{O} + \text{KHCO}_3$ binary systems, 5% for liquid phase species mole fractions in $\text{H}_2\text{O} + \text{K}_2\text{CO}_3$ binary and 10% in $\text{H}_2\text{O} + \text{KHCO}_3$ binary.
- 5% for mean ionic activity coefficient data, 15% for osmotic coefficient data, 5% for heat capacity data, and 5% for excess enthalpy data in $\text{H}_2\text{O} + \text{K}_2\text{CO}_3$ and $\text{H}_2\text{O} + \text{KHCO}_3$ binary systems. The liquid phase species mole fractions are set error free.
- 10% for CO_2 partial pressure, 5% for total pressure, 5% for liquid phase species mole fractions, and 0.01 for vapor phase species mole fractions in $\text{H}_2\text{O} + \text{K}_2\text{CO}_3 + \text{CO}_2$ ternary system for CO_2 solubility data.
- 5% for liquid phase mole fractions of K_2CO_3 and KHCO_3 in their respective salt solubility data.

Table 5 reports the weight assigned to each experimental data set depending upon the significance and quality of the data. The regressed values of binary interaction parameters and thermodynamic constants for salts are summarized in Table 6 and Table 3 respectively. Residual root-mean-square-error (RRMSE) as described by Yan and Chen [27] is the minimization objective function used in performing data regression in all regression cases. RRMSE is defined as:

$$\text{RRMSE} = \sqrt{\frac{\sum_{i=1}^k \sum_{j=1}^m [(Z_{ij} - ZM_{ij})/\sigma_{ij}]^2}{k-n}} \quad (6)$$

where ZM is the experimentally measured value, Z is the calculated value, σ is the standard deviation of the data, i is the index of the data point, j is the measured variable for each data point (such as temperature, pressure, or composition), k is the total number of data points, m is the total number of measured variables for each data point, and n is the total number of adjustable parameters.

4. Results and Discussion

4.1 $H_2O + K_2CO_3$ binary system

Figures 2 to 6 show the comparisons between the experimental data and the model correlation results for various thermodynamic and calorimetric properties for aqueous K_2CO_3 solution.

Figure 2 shows an excellent agreement between the smoothed H_2O vapor pressure data [30] and the model results for the K_2CO_3 concentration up to saturation and the temperature range of 273.15 K to 473.15 K. The MRD is 2.37%. The model extrapolations up to 523.15 K are also in satisfactory agreement with the data. Significant deviations start to develop above 573.15 K.

Figure 3 shows the comparison between the experimental molality-scale mean ionic activity coefficient data [31, 32] and the model results at 298.15 K. With an overall MRD of ~9.7%, a satisfactory agreement is achieved between the model results and the experimental data up to ~6 molal. Note that the experimental mean ionic activity coefficient data are actually smoothed data with the Pitzer model [31, 32] while the Pitzer model is considered valid up to ionic strength of 6 molal [14, 15]. This is supported by a recent study showing the Pitzer model extrapolations above ionic strength of 6 molal diverge from the predictions based on molecular simulations and Kirkwood-Buff theory [37]. In other words, we consider the experimental data less reliable at high K_2CO_3 concentrations. Figure 4 shows the comparison between the experimental osmotic coefficient data [31, 32] and the model results at 298.15 K. The MRD is slightly less than 8%. Given that the experimental data were smoothed with the Pitzer equation and the model captures well the experimental water vapor pressure data [30] across all concentrations as shown in Figure 2, following Gibbs-Duhem relationship, we consider the model results for mean ionic activity coefficient and osmotic coefficient acceptable.

Figure 5 shows a reasonable agreement between the experimental excess enthalpy data at 298.15 K [33] and the model results for dilute K_2CO_3 solutions. It is interesting that, while the model captures the rather sparse enthalpy data points well, it suggests a S-shape concentration dependence for the excess enthalpy. Figure 6 illustrates the comparison between the smoothed heat capacity data [30] and the model results in the temperature range of 323.15 to 423.15 K. An excellent agreement between the model results and the data is observed at temperatures in the range of 323.15 to 393.15 K. Notable deviations are observed at higher temperatures. However, with the overall MRD of 1.28%, we consider the model results satisfactory.

4.2 $H_2O + KHCO_3$ binary system

Figures 7 to 9 illustrate the comparisons between the experimental data and the model results for the aqueous KHCO_3 solution. Figure 7 shows an excellent agreement between the experimental molality-scale mean ionic activity coefficient data [31] and the model results whereas Figure 8 shows an excellent agreement between the osmotic coefficient data [31] and the model results, both at 298.15 K and up to 2.5 molal KHCO_3 concentration. Figure 9 compares the experimental heat capacity data [30] with the model results in the temperature range of 283.15 to 433.15 K. While the experimental data seem scattered and the model results deviate slightly from the data, the overall MRD is less than 4%.

4.3 $\text{H}_2\text{O} + \text{K}_2\text{CO}_3 + \text{CO}_2$ ternary system

Figures 10 to 13 illustrate the model results for CO_2 solubility over different K_2CO_3 concentrations, temperatures, and CO_2 loadings. Figure 10 shows an excellent agreement between the experimental data of Tosh et al. [8] and Korbutova et al. [34] and the model results for CO_2 partial pressure over a 20 wt.% K_2CO_3 solution, the CO_2 loading range of 0 to 1, and temperature varying from 323.15 to 403.15 K. Figure 11 illustrates that the model accurately represents the experimental data from multiple sources [4, 8, 34, 35] over a 30 wt.% K_2CO_3 solution in the CO_2 loading range of 0 to 1 and temperature varying from 323.15 to 403.15 K. Figure 12 presents a good agreement between the model results and the experimental data of Tosh et al. [8] over a 40 wt.% K_2CO_3 solution in the CO_2 loading range of 0 to 1 and temperature varying from 323.15 to 413.15 K. We further investigate the model results for CO_2 solubility at ultrahigh CO_2 loadings (>1). Figure 13 shows an excellent agreement between the model results for total pressure and the experimental data of Kamps et al. [7] at low K_2CO_3 concentrations of ~0.4 to 0.5 molal, high CO_2 loading of 0.9 to 3.4, and temperature from 313.15 to 393.15 K. Figure 14 shows an excellent agreement between the model results and the experimental data of

Kamps et al. [7] at high K_2CO_3 concentration of 1.71 molal, CO_2 loading of 0.4 to 1.5, and temperature from 313.15 to 393.15 K. Figure 14 also shows the experimental data of Bohloul et al. at 20 wt.% (~ 1.81 molal) K_2CO_3 at 333.15 K. The data are clearly outliers as they deviate completely from the general trend of CO_2 solubility data as captured by this work.

4.4 Precipitating salts

Figure 15 shows that the model accurately represents the experimental salt solubility data reported by Seidell [25] and Moore et al. [26] for K_2CO_3 salts. It has been reported in the literature that in the temperature range of 298 to 429 K, upon saturation, K_2CO_3 precipitates out as hydrated potassium carbonate ($\text{K}_2\text{CO}_3 \cdot \frac{3}{2} \text{H}_2\text{O}$) salt [25, 26] as represented by reaction R7. However, at temperatures above 429 K, it was experimentally observed that the shape of the crystal changed from a small granular shape to a larger, more cylindrical shape [26]. This behavior coincides with the change in slope of the salt solubility above 429 K, thereby suggesting a change in the crystal form at such elevated temperatures. To the best of our knowledge the crystal form at temperatures above 429 K has not been reported yet. This work assumes the hydrated K_2CO_3 salt lose its hydration water and the crystal form is an anhydrous K_2CO_3 salt as represented by reaction R9.



The thermodynamic constants for the anhydrous K_2CO_3 salt are then identified from regression of the solubility data in the range of 429 K to 473 K by Moore et al. [26]. Figure 15 also shows an excellent agreement between the experimental salt solubility data by Seidell [25] and the model results for the solubility of KHCO_3 salt.

5. Conclusion

A rigorous and comprehensive thermodynamic representation has been successfully developed with symmetric eNRTL activity coefficient model for $\text{H}_2\text{O} + \text{K}_2\text{CO}_3$ binary, $\text{H}_2\text{O} + \text{KHCO}_3$ binary, and $\text{H}_2\text{O} + \text{K}_2\text{CO}_3 + \text{CO}_2$ ternary systems. The model covers the K_2CO_3 concentration range from pure H_2O to salt saturation, the temperature range of 273.15 to 473.15 K, and the CO_2 loading range of 0 to 3.6. The model provides a thermodynamically consistent representation of various thermodynamic and calorimetric properties such as vapor pressure, mean ionic activity coefficient, osmotic coefficient, heat capacity, excess enthalpy and salt solubility. The model should be a very useful tool in the process simulation and design of CO_2 capture units involving hot, concentrated K_2CO_3 solutions at elevated temperatures and pressures.

Acknowledgment

The authors gratefully acknowledge the financial support of the Jack Maddox Distinguished Engineering Chair Professorship in Sustainable Energy sponsored by the J.F Maddox Foundation.

References

- [1] H. E. Benson, J. H. Field, and R. M. Jimeson, "CO₂ absorption: employing hot potassium carbonate solutions," *Chem. Eng. Prog.;(United States)*, vol. 50, no. 7, pp. 356-364, 1954.
- [2] A. Lee, M. Wolf, N. Kromer, K. A. Mumford, N. J. Nicholas, S. E. Kentish, and G. W. Stevens, "A study of the vapour–liquid equilibrium of CO₂ in mixed solutions of potassium carbonate and potassium glycinate," *International Journal of Greenhouse Gas Control*, vol. 36, pp. 27-33, 2015.
- [3] A. Lee, K. A. Mumford, Y. Wu, N. Nicholas, and G. W. Stevens, "Understanding the vapour–liquid equilibrium of CO₂ in mixed solutions of potassium carbonate and potassium glycinate," *International Journal of Greenhouse Gas Control*, vol. 47, pp. 303-309, 2016.
- [4] K. Endo, Q. S. Nguyen, S. E. Kentish, and G. W. Stevens, "The effect of boric acid on the vapour liquid equilibrium of aqueous potassium carbonate," *Fluid Phase Equilibria*, vol. 309, no. 2, pp. 109-113, 2011.
- [5] T. N. G. Borhani, A. Azarpour, V. Akbari, S. R. W. Alwi, and Z. A. Manan, "CO₂ capture with potassium carbonate solutions: A state-of-the-art review," *International Journal of Greenhouse Gas Control*, vol. 41, pp. 142-162, 2015.
- [6] O. Erga, O. Juliussen, and H. Lidal, "Carbon dioxide recovery by means of aqueous amines," *Energy Conversion and Management*, vol. 36, no. 6-9, pp. 387-392, 1995.
- [7] Á. Pérez-Salado Kamps, E. Meyer, B. Rumpf, and G. Maurer, "Solubility of CO₂ in aqueous solutions of KCl and in aqueous solutions of K₂CO₃," *Journal of Chemical & Engineering Data*, vol. 52, no. 3, pp. 817-832, 2007.
- [8] J. S. Tosh, J. H. Field, H. E. Benson, and R. B. Anderson, "Equilibrium pressures of hydrogen sulfide and carbon dioxide over solutions of potassium carbonate," Bureau of Mines, Washington, DC (USA); Bureau of Mines, Pittsburgh, PA (USA)1959.
- [9] S.-B. Park, C.-S. Shim, H. Lee, and K.-H. Lee, "Solubilities of carbon dioxide in the aqueous potassium carbonate and potassium carbonate-poly (ethylene glycol) solutions," *Fluid Phase Equilibria*, vol. 134, no. 1-2, pp. 141-149, 1997.
- [10] J. T. Cullinane and G. T. Rochelle, "Carbon dioxide absorption with aqueous potassium carbonate promoted by piperazine," *Chemical Engineering Science*, vol. 59, no. 17, pp. 3619-3630, 2004.
- [11] S. Shen, X. Feng, R. Zhao, U. K. Ghosh, and A. Chen, "Kinetic study of carbon dioxide absorption with aqueous potassium carbonate promoted by arginine," *Chemical Engineering Journal*, vol. 222, pp. 478-487, 2013.
- [12] H. Thee, N. J. Nicholas, K. H. Smith, G. da Silva, S. E. Kentish, and G. W. Stevens, "A kinetic study of CO₂ capture with potassium carbonate solutions promoted with various amino acids: glycine, sarcosine and proline," *International Journal of Greenhouse Gas Control*, vol. 20, pp. 212-222, 2014.
- [13] C.-C. Chen, H. I. Britt, J. F. Boston, and L. B. Evans, "Extension and application of the pitzer equation for vapor-liquid equilibrium of aqueous electrolyte systems with molecular solutes," *AIChE Journal*, vol. 25, no. 5, pp. 820-831, 1979.
- [14] K. S. Pitzer, "Thermodynamics of electrolytes. I. Theoretical basis and general equations," *The Journal of Physical Chemistry*, vol. 77, no. 2, pp. 268-277, 1973.
- [15] K. S. Pitzer, "Ion interaction approach: theory and data correlation," *Activity coefficients in electrolyte solutions*, CRC Press, Boca Raton, pp. 75-154, 1991.
- [16] M. R. Bohloul, M. A. Sadeghabadi, S. M. Peyghambarzadeh, and M. R. Dehghani, "CO₂ absorption using aqueous solution of potassium carbonate: Experimental measurement and thermodynamic modeling," *Fluid Phase Equilibria*, vol. 447, pp. 132-141, 2017.
- [17] J. T. Cullinane and G. T. Rochelle, "Thermodynamics of aqueous potassium carbonate, piperazine, and carbon dioxide," *Fluid Phase Equilibria*, vol. 227, no. 2, pp. 197-213, 2005.

- [18] C.-C. Chen and L. B. Evans, "A local composition model for the excess Gibbs energy of aqueous electrolyte systems," *AIChE Journal*, vol. 32, no. 3, pp. 444-454, 1986.
- [19] M. D. Hilliard, "A predictive thermodynamic model for an aqueous blend of potassium carbonate, piperazine, and monoethanolamine for carbon dioxide capture from flue gas," *University of Texas at Austin*, Doctoral dissertation, 2008.
- [20] Y. Zhang and C.-C. Chen, "Thermodynamic modeling for CO₂ absorption in aqueous MDEA solution with electrolyte NRTL model," *Industrial & Engineering Chemistry Research*, vol. 50, no. 1, pp. 163-175, 2010.
- [21] Y. Zhang, H. Que, and C.-C. Chen, "Thermodynamic modeling for CO₂ absorption in aqueous MEA solution with electrolyte NRTL model," *Fluid Phase Equilibria*, vol. 311, pp. 67-75, 2011.
- [22] L. Zong and C.-C. Chen, "Thermodynamic modeling of CO₂ and H₂S solubilities in aqueous DIPA solution, aqueous sulfolane-DIPA solution, and aqueous sulfolane-MDEA solution with electrolyte NRTL model," *Fluid Phase Equilibria*, vol. 306, no. 2, pp. 190-203, 2011.
- [23] H. Que and C.-C. Chen, "Thermodynamic modeling of the NH₃-CO₂-H₂O system with electrolyte NRTL model," *Industrial & Engineering Chemistry Research*, vol. 50, no. 19, pp. 11406-11421, 2011.
- [24] J. Gross and G. Sadowski, "Perturbed-chain SAFT: An equation of state based on a perturbation theory for chain molecules," *Industrial & Engineering Chemistry Research*, vol. 40, no. 4, pp. 1244-1260, 2001.
- [25] A. Seidell, "Solubilities of Inorganic and Metal Organic Compounds," *Van Nostrand Company, Inc., New York*, 1953.
- [26] R. C. Moore, R. E. Mesmer, and J. M. Simonson, "Solubility of potassium carbonate in water between 384 and 529 K measured using the synthetic method," *Journal of Chemical & Engineering Data*, vol. 42, no. 6, pp. 1078-1081, 1997.
- [27] Y. Yan and C.-C. Chen, "Thermodynamic modeling of CO₂ solubility in aqueous solutions of NaCl and Na₂SO₄," *The Journal of Supercritical Fluids*, vol. 55, no. 2, pp. 623-634, 2010.
- [28] Y. Song and C.-C. Chen, "Symmetric electrolyte nonrandom two-liquid activity coefficient model," *Industrial & Engineering Chemistry Research*, vol. 48, no. 16, pp. 7788-7797, 2009.
- [29] S. K. Bhattacharia and C.-C. Chen, "Thermodynamic modeling of KCl+ H₂O and KCl+ NaCl+ H₂O systems using electrolyte NRTL model," *Fluid Phase Equilibria*, vol. 387, pp. 169-177, 2015.
- [30] G. G. Aseyev, "Electrolytes: equilibria in solutions and phase equilibria," *Calculation of Multicomponent Systems and Experimental Data on the Activities of Water, Vapor Pressures, and Osmotic Coefficients*, Begell House, New York, 1999.
- [31] R. N. Roy, J. J. Gibbons, R. Williams, L. Godwin, G. Baker, J. M. Simonson, and K. S. Pitzer, "The thermodynamics of aqueous carbonate solutions II. mixtures of potassium carbonate, bicarbonate, and chloride," *The Journal of Chemical Thermodynamics*, vol. 16, no. 4, pp. 303-315, 1984.
- [32] M. Sarbar, A. K. Covington, R. L. Nuttall, and R. N. Goldberg, "Activity and osmotic coefficients of aqueous potassium carbonate," *The Journal of Chemical Thermodynamics*, vol. 14, no. 7, pp. 695-702, 1982.
- [33] D. D. Wagman, W. H. Evans, V. B. Parker, R. H. Schumm, I. Halow, B. M. Sylvia, C. L. Kenneth, and N. L. Ralph, "The NBS tables of chemical thermodynamic properties. Selected values for inorganic and C1 and C2 organic substances in SI units," *Journal of Physical and Chemical Reference Data*, vol. 11, Supplement No. 2, 1982.
- [34] Z. V. Korbutova, Y. G. Karpova, and I. L. Leites, "Solubility of carbon dioxide in aqueous solutions of potassium carbonate," *Khimicheskaya Promyshlennost (Moscow, Russian Federation)*, vol. 12, pp. 721-723, 1980.

- [35] H. Jo, M.-g. Lee, B. Kim, H.-J. Song, H. Gil, and J. Park, "Density and solubility of CO₂ in aqueous solutions of (potassium carbonate+ sarcosine) and (potassium carbonate+ pipecolic acid)," *Journal of Chemical & Engineering Data*, vol. 57, no. 12, pp. 3624-3627, 2012.
- [36] "Aspen Properties V8.8," *Aspen Technoloy, Inc.: Burlington, MA*, 2015.
- [37] N. Hossain, A. Ravichandran, R. Khare, and C. C. Chen, "Revisiting electrolyte thermodynamic models: Insights from molecular simulations," *AIChE Journal*, vol. 64, no. 10, pp. 3728-3734, 2018.

List of Tables

Table 1: PC-SAFT equation of state model parameters

Components	H ₂ O	CO ₂
Source	Gross and Sadowski [24]	Gross and Sadowski [24]
Segment number parameter, m	1.0656	2.5692
Segment size parameter, σ	3.0007	2.5637
Segment energy parameter, ε (K)	366.51	152.1
Association energy parameter, ε^{AB} (K)	2500.7	0
Association energy parameter, k^{AB} (Å ³)	0.034868	0

Table 2. Thermodynamic constants for molecules and ions at 298.15 K and 0.1 MPa

Components	$\Delta_f H_{m,298.15}^{ig}$	$\Delta_f H_{i,298.15}^{\infty,aq}$	$\Delta_f G_{m,298.15}^{ig}$	$\Delta_f G_{i,298.15}^{\infty,aq}$	$C_{p,m}^{ig}$
	kJ/mol	kJ/mol	kJ/mol	kJ/mol	J/mol/K
H ₂ O	-241.818 ^a		-228.572 ^a		33.577 ^a
K ⁺		-252.38 ^b		-283.27 ^b	-21.8 ^b
HCO ₃ ⁻		-691.99 ^b		-586.77 ^b	-29.26 ^b
CO ₃ ²⁻		-677.14 ^b		-527.81 ^b	-39.71 ^b

$\Delta_f H_{m,298.15}^{ig}$ and $\Delta_f G_{m,298.15}^{ig}$ are the ideal gas enthalpy of formation and Gibbs free energy of molecular species *m* at 298.15 K, whereas $\Delta_f H_{i,298.15}^{\infty,aq}$ and $\Delta_f G_{i,298.15}^{\infty,aq}$ are the enthalpy of formation and Gibbs free energy of ionic species *i* at the aqueous phase infinite dilution reference state.

^a Parameters taken from Aspen Plus Databank [36], ^b Parameters taken from Wagman et al. [33]

Table 3. Thermodynamic constants for solids precipitated at 298.15 K and 0.1 MPa

Solid	$\Delta_f H_k^o$ [33]	$\Delta_f H_k^o$ Est ^a	$\Delta_f G_k^o$ [33]	$\Delta_f G_k^o$ Est ^a	C_p^o [33]	C_p^o Est ^a
	kJ/mol	kJ/mol	kJ/mol	kJ/mol	J/mol/K	J/mol/K
K ₂ CO ₃ . ₂ ³ H ₂ O(cr)	-1609.2	-1617.2 ± 0.073	-1432.5	-1435.2 ± 0.007		80.6 ± 2.916
K ₂ CO ₃ (cr)	-1151.02	-1158.8 ± 3.490	-1063.5	-1066.8 ± 1.167	114.43	
KHCO ₃ (cr)	-963.2	-998.5 ± 0.024	-863.5	-868.5 ± 0.003		-491.5 ± 0.082

^a Est are the values obtained in this work

Table 4. Summary of model parameters

Parameter	Component	Source
PC-SAFT EoS	H ₂ O, CO ₂	Aspen Plus databank [36]
Antoine equation	H ₂ O, CO ₂	Aspen Plus databank [36]
Henry's constant	CO ₂ in H ₂ O	Yan and Chen [27]
eNRTL binary interaction parameters τ_{ij}	CO ₂ -H ₂ O pair	Yan and Chen [27]
	H ₂ O-(K ⁺ , CO ₃ ²⁻) pair	Regression from vapor pressure, mean-ionic activity coefficient, osmotic coefficient, excess enthalpy and heat capacity data for H ₂ O + K ₂ CO ₃ system
	H ₂ O-(K ⁺ , HCO ₃ ⁻) pair, (K ⁺ , CO ₃ ²⁻)-(K ⁺ , HCO ₃ ⁻) pair, CO ₂ -(K ⁺ , CO ₃ ²⁻) pair, CO ₂ -(K ⁺ , HCO ₃ ⁻) pair	Regression from vapor pressure, mean-ionic activity coefficient, osmotic coefficient and heat capacity data for H ₂ O + KHCO ₃ system and VLE data for H ₂ O + K ₂ CO ₃ + CO ₂ system
$\Delta_f H_{m,298.15}^{ig}, \Delta_f G_{m,298.15}^{ig}, C_{p,m}^{ig}$	H ₂ O, CO ₂	Aspen Plus databank [36]
$\Delta_f H_{i,298.15}^{\infty,aq}, \Delta_f G_{i,298.15}^{\infty,aq}, C_{p,i}^{\infty,aq}$	K ⁺ , H ₃ O ⁺ , OH ⁻ , HCO ₃ ⁻ , CO ₃ ²⁻	Aspen Plus databank [36]
$\Delta_f H_k^o, \Delta_f G_k^o, C_p^o$	K ₂ CO ₃ (cr), KHCO ₃ (cr), K ₂ CO ₃ .1.5H ₂ O(cr)	Regression from salt solubility data for H ₂ O + K ₂ CO ₃ and H ₂ O + KHCO ₃ systems

Table 5. Experimental data used in different cases of regression

Source	Data type	Temperature (K)	Concentration	No. of data pts.	MRD (%)	Weight
<i>H₂O + K₂CO₃ binary system</i>						
Aseyev [30]	c _p	283-463	2-50 wt.% K ₂ CO ₃	450 (100)	1.28	1
Aseyev [30]	TPxy ^a	298-623	2-76 wt.% K ₂ CO ₃	1205 (219)	2.37	1
Roy et al. [31]	$\gamma_{\pm m}^*$	298	0.001-8.1 molal K ₂ CO ₃	29	9.66	1
	ϕ				7.89	0.5
Sarbar et al. [32]	$\gamma_{\pm m}^*$	298	0.001-8.1 molal K ₂ CO ₃	57	9.76	1
	ϕ				7.80	0.5
Wagman et al. [33]	Enthalpy of solution	298	0.0001-0.09 mole frac. K ₂ CO ₃	15	51.83	1
Seidell [25]	Salt Solubility	273-403	7.6-14.2 molal K ₂ CO ₃	15	0.81	1
Moore et al. [26]	Salt Solubility	384-529	11.8-19.1 molal K ₂ CO ₃	21 (17)	3.16	0.5
<i>H₂O + KHCO₃ binary system</i>						
Aseyev [30]	c _p	278-473	4-22 wt.% KHCO ₃	351 (59)	3.34	1
Aseyev [30]	TPxy ^a	298	2-20 wt.% KHCO ₃	11	0.92	1
Roy et al. [31]	$\gamma_{\pm m}^*$	298	0.001-2 molal KHCO ₃	17	0.88	1
	ϕ				0.29	1
Seidell [25]	Salt Solubility	273-343	2.3-7.6 molal KHCO ₃	8	0.83	1
<i>H₂O + K₂CO₃ + CO₂ ternary system</i>						
Tosh et al. [8]	TPxy	343-413	20-40 wt.% K ₂ CO ₃ CO ₂ loading 0-1	148	5.75	1
Korbutova et al. [34]	TPxy	313-353	20-30 wt.% K ₂ CO ₃ CO ₂ loading 0.1-0.42	65	13.87	1
Park et al. [9]	TPxy	298, 323	5 wt.%, 10 wt.%	28	33.87	10 ⁻⁵

			CO_2 loading 0.7-1.8			
Kamps et al. [7]	TPxy	313, 353, 393	0.43-1.7 molal K_2CO_3 CO_2 loading 0.7-3.6	41	11.76	1
Endo et al. [4]	TPxy	323, 343	30 wt.% K_2CO_3 CO_2 loading 0.15-0.40	21	16.78	1
Jo et al. [35]	TPxy	373, 393	30 wt.% K_2CO_3 CO_2 loading 0.1-1.0	22	24.86	1
Bohloul et al. [16]	TPxy	313, 323, 333	15, 20 and 30 wt.% K_2CO_3 CO_2 loading 0.40-1.25	87	112.25*	0

^a H_2O vapor pressure data only. *Data set excluded from regression. Values in parenthesis: Actual number of data points used in regression.

Table 6. Binary interaction parameters for the $H_2O + K_2CO_3 + CO_2$ ternary system

Component <i>i</i>	Component <i>j</i>	<i>a_{ij}</i>	<i>b_{ij}</i>	<i>c_{ij}</i>	τ_{ij}^a (at 298.15 K)	Source
H_2O	(H_3O^+, OH^-)	8.045	0	0	8.045	Aspen Plus Databank [36]
(H_3O^+, OH^-)	H_2O	-4.072	0	0	-4.072	
H_2O	(H_3O^+, CO_3^{2-})	8.045	0	0	8.045	
(H_3O^+, CO_3^{2-})	H_2O	-4.072	0	0	-4.072	
H_2O	(H_3O^+, HCO_3^-)	8.045	0	0	8.045	
(H_3O^+, HCO_3^-)	H_2O	-4.072	0	0	-4.072	
CO_2	(H_3O^+, OH^-)	8.045	0	0	8.045	
(H_3O^+, OH^-)	CO_2	-4.072	0	0	-4.072	
CO_2	(H_3O^+, CO_3^{2-})	8.045	0	0	8.045	
(H_3O^+, CO_3^{2-})	CO_2	-4.072	0	0	-4.072	
CO_2	(H_3O^+, HCO_3^-)	8.045	0	0	8.045	
(H_3O^+, HCO_3^-)	CO_2	-4.072	0	0	-4.072	
H_2O	(K^+, OH^-)	7.840	773.4	-5.852	10.434	
(K^+, OH^-)	H_2O	-4.259	-305.6	4.754	-5.284	
H_2O	(K^+, CO_3^{2-})	7.362 ± 0.095	648.5 ± 20.2	2.988 ± 2.158	9.537	This work
(K^+, CO_3^{2-})	H_2O	-4.196 ± 0.032	-147.8 ± 7.4	1.817 ± 0.722	-4.692	
H_2O	(K^+, HCO_3^-)	0.542 ± 0.287	2263.2 ± 78.2	-3.171 ± 0.736	8.133	
(K^+, HCO_3^-)	H_2O	-4.140 ± 0.161	63.5 ± 11.2	0.304 ± 0.091	-3.927	
(K^+, CO_3^{2-})	(K^+, HCO_3^-)	16.209 ± 2.578	-4780.5 ± 856.9	0	0.175	
(K^+, HCO_3^-)	(K^+, CO_3^{2-})	-2.308 ± 0.397	452.2 ± 125.3	0	-0.791	
CO_2	(K^+, HCO_3^-)	14.629 ± 3.312	0	0	14.629	
(K^+, HCO_3^-)	CO_2	-2.834 ± 1.075	0	0	-2.834	
CO_2	(K^+, CO_3^{2-})	0	0	0	0	
(K^+, CO_3^{2-})	CO_2	-5.446 ± 1.281	0	0	-5.446	

$$^a \tau_{ij} = a_{ij} + \frac{b_{ij}}{T} + c_{ij} \left(\frac{T_{ref}-T}{T} + \ln\left(\frac{T}{T_{ref}}\right) \right), \alpha_{ij} = 0.2$$

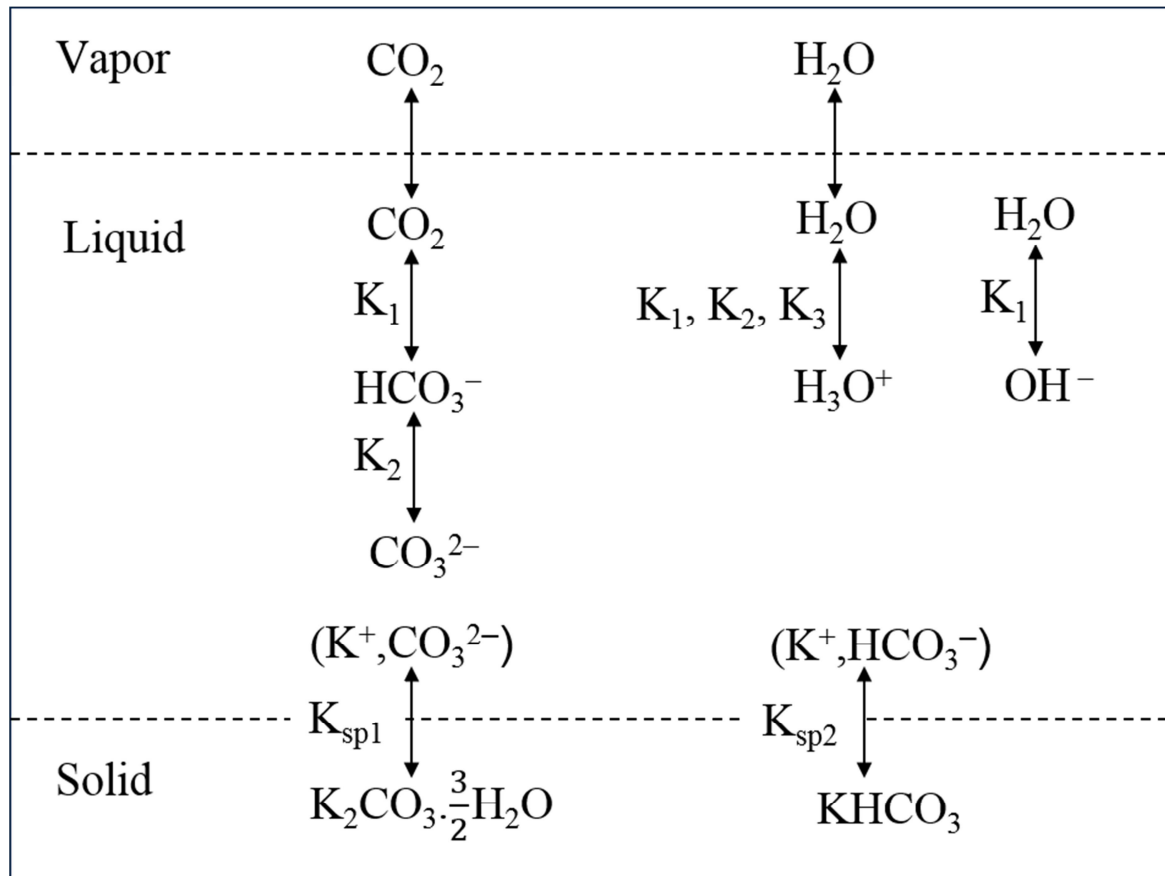


Figure 1. Solution chemistry and speciation in $\text{H}_2\text{O} + \text{K}_2\text{CO}_3 + \text{CO}_2$ ternary system

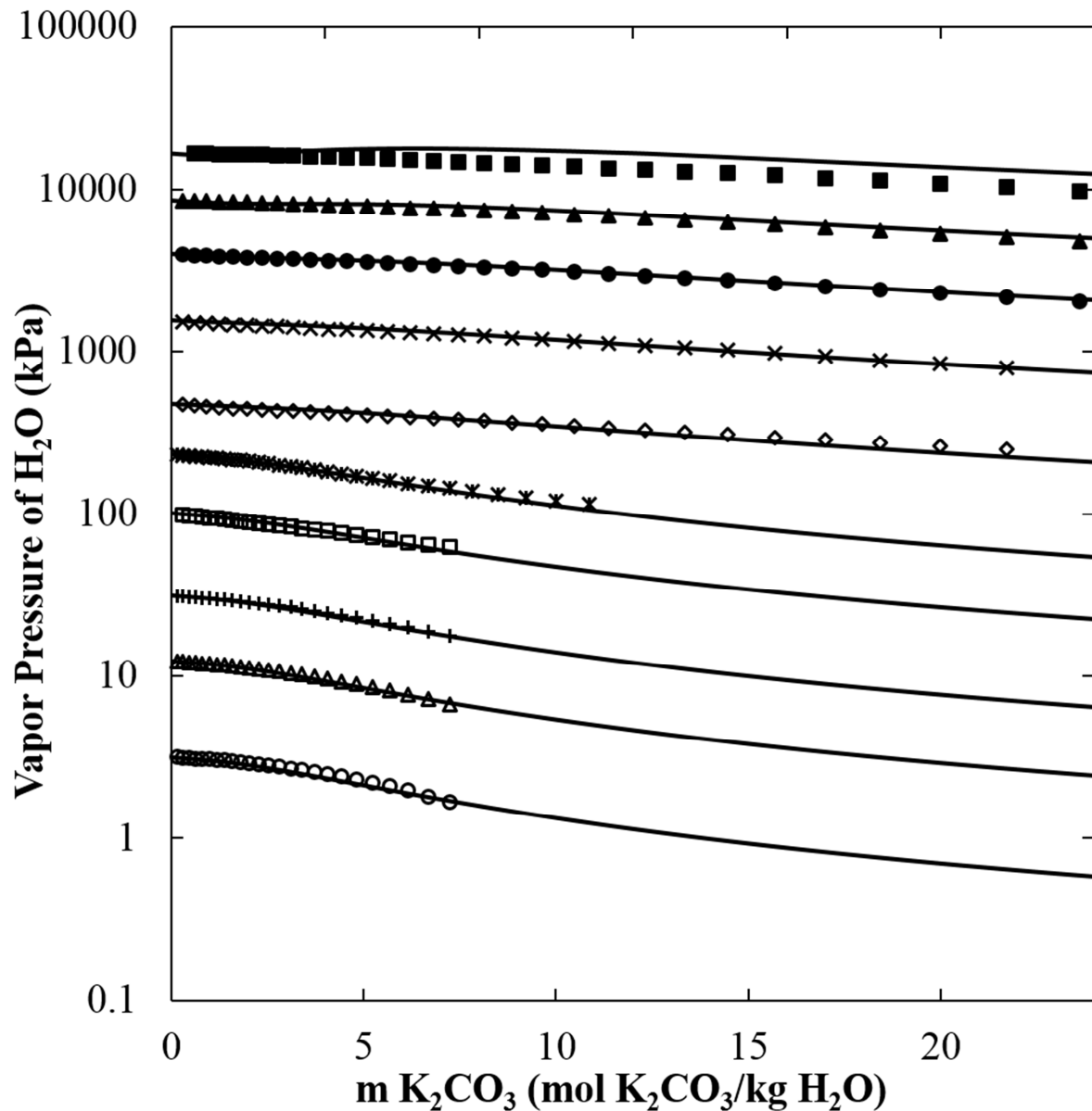


Figure 2. H₂O vapor pressure of aqueous K₂CO₃ solution with experimental data [30] in symbols and model results in lines (—) at 298.15 K (○), 323.15 K (△), 343.15 K (+), 373.15 K (□), 398.15 K (*), 428.15 K (◊), 473.15 K (×), 523.15 K (●), 573.15 K (▲), 623.15 K (■)

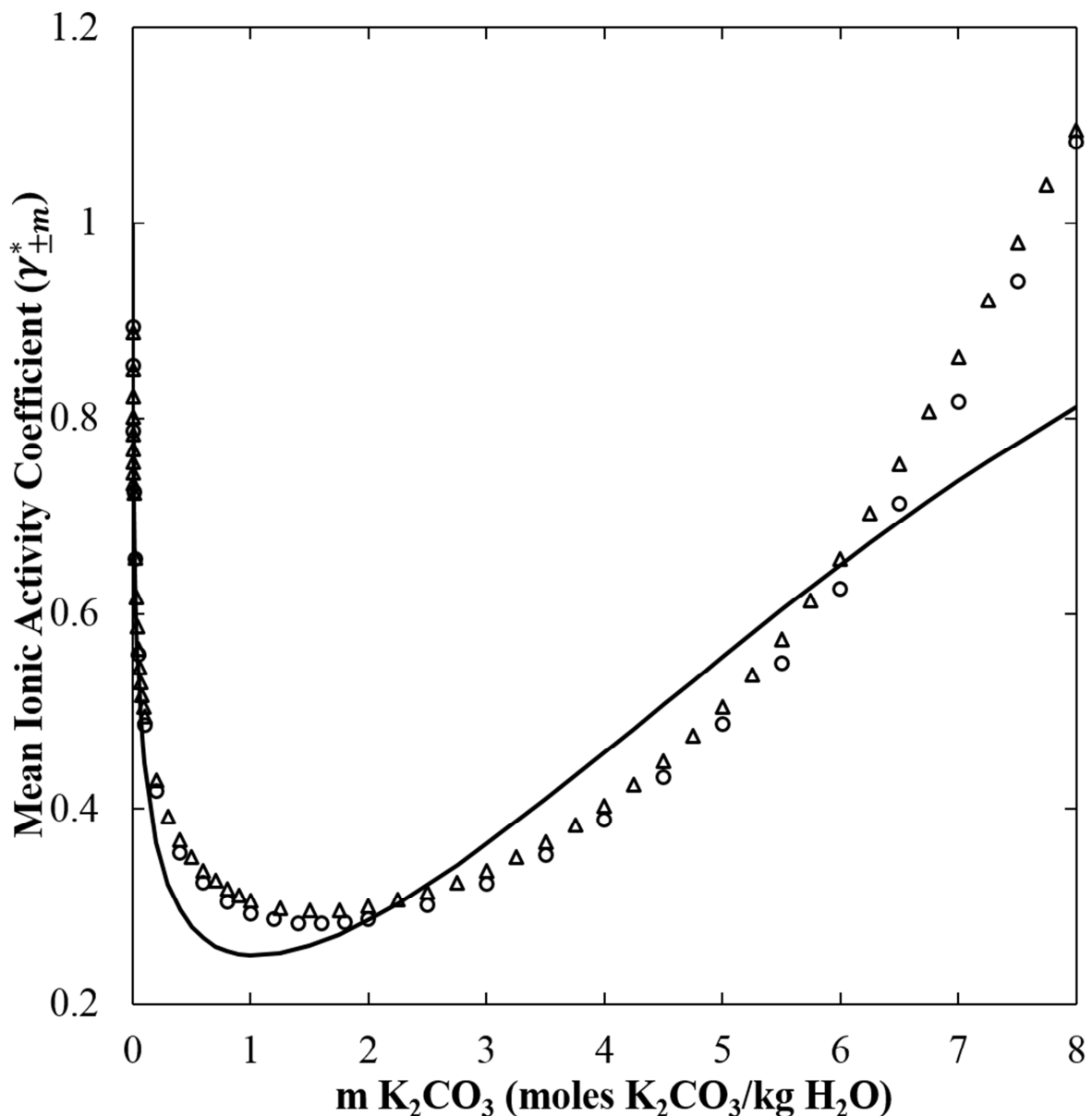


Figure 3. Molality-scale mean ionic activity coefficient of aqueous K_2CO_3 solution with experimental data [31] (○) [32] (△) and model results (—) at 298.15 K

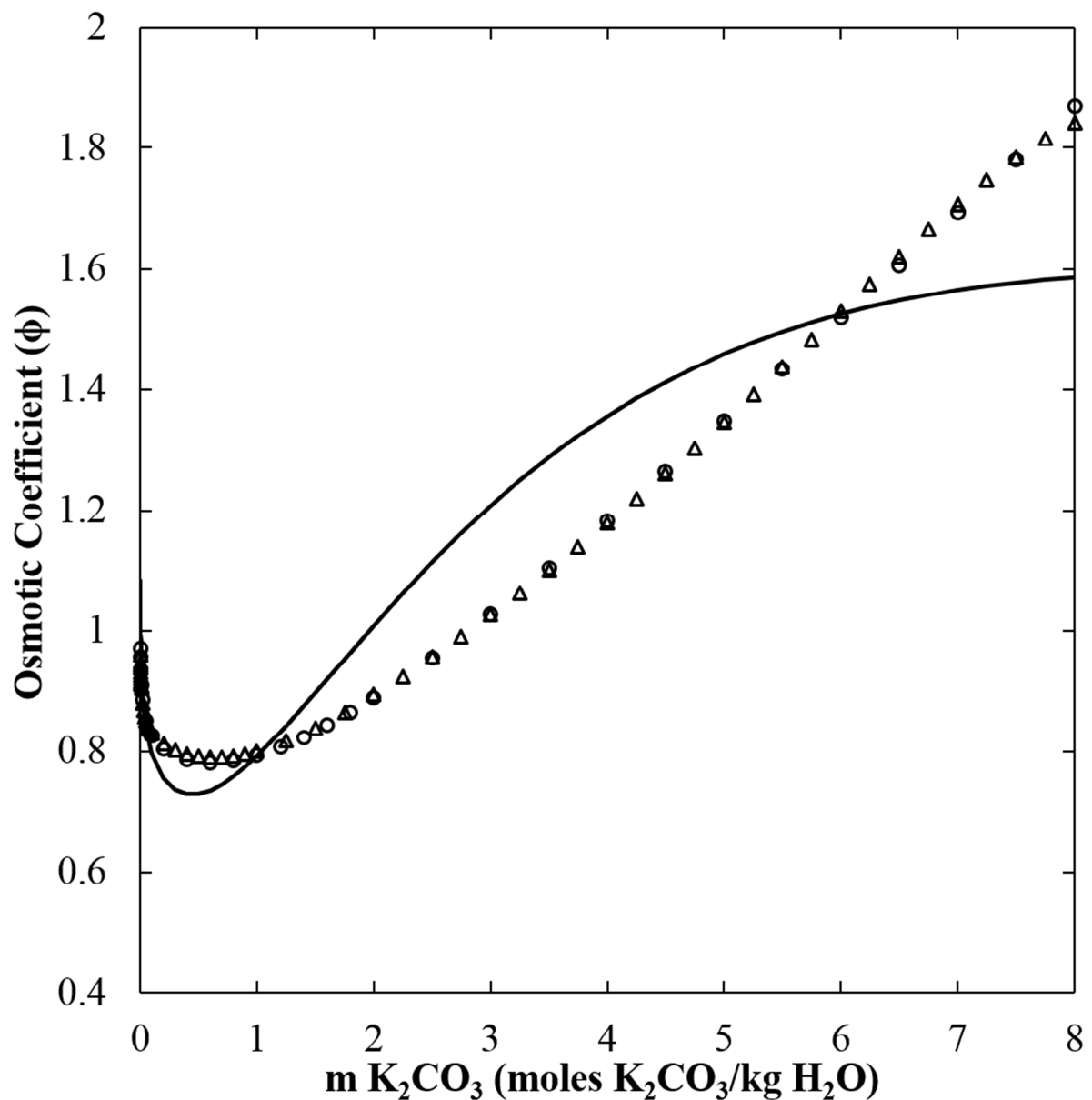


Figure 4. Osmotic coefficient of aqueous K_2CO_3 solution with experimental data [31] (●) [32] (△) and model results (—) at 298.15 K

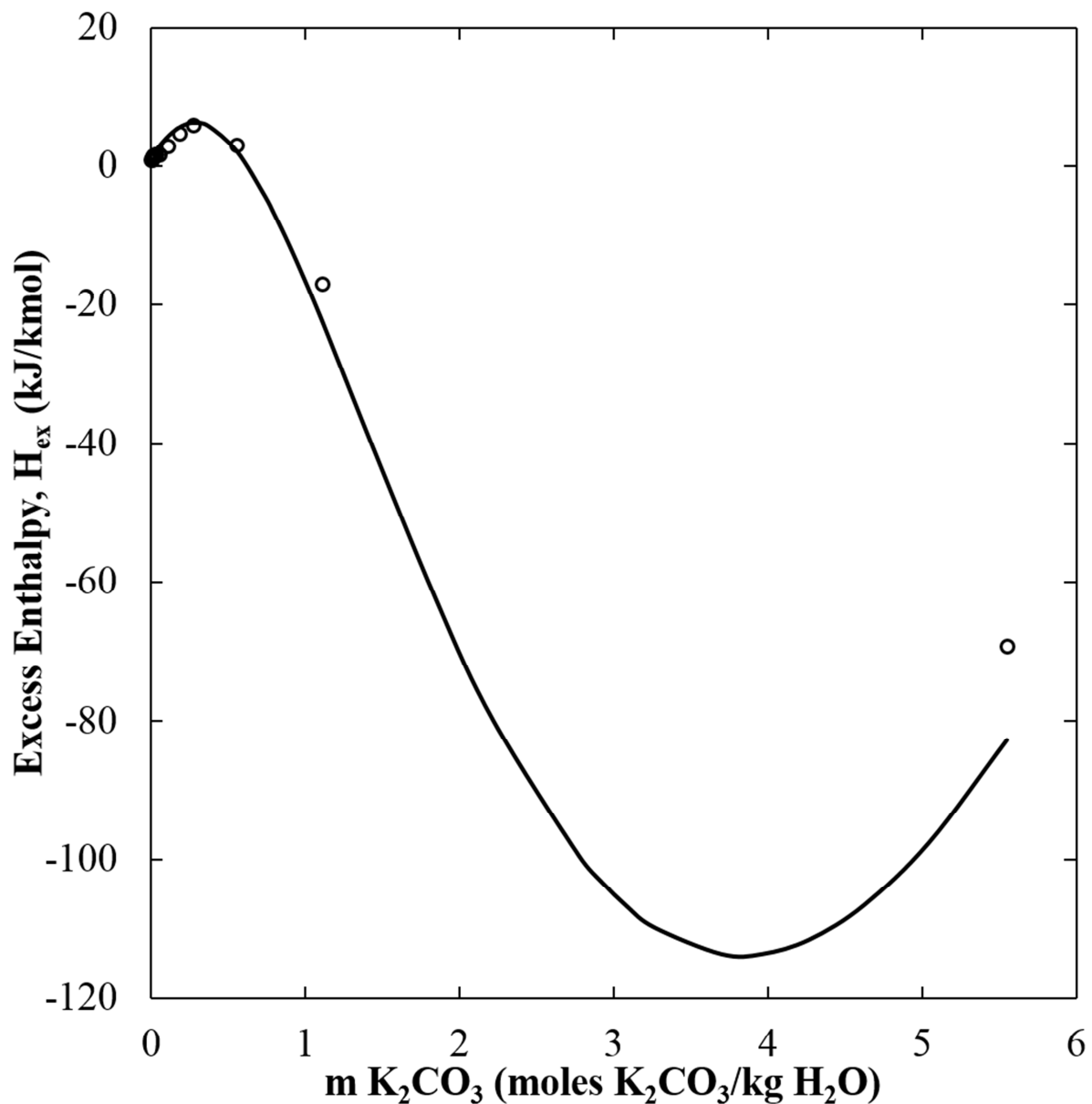


Figure 5. Excess enthalpy of aqueous K_2CO_3 solution with experimental data [33] (\bullet) and model results (—) at 298.15 K and 0.1 MPa

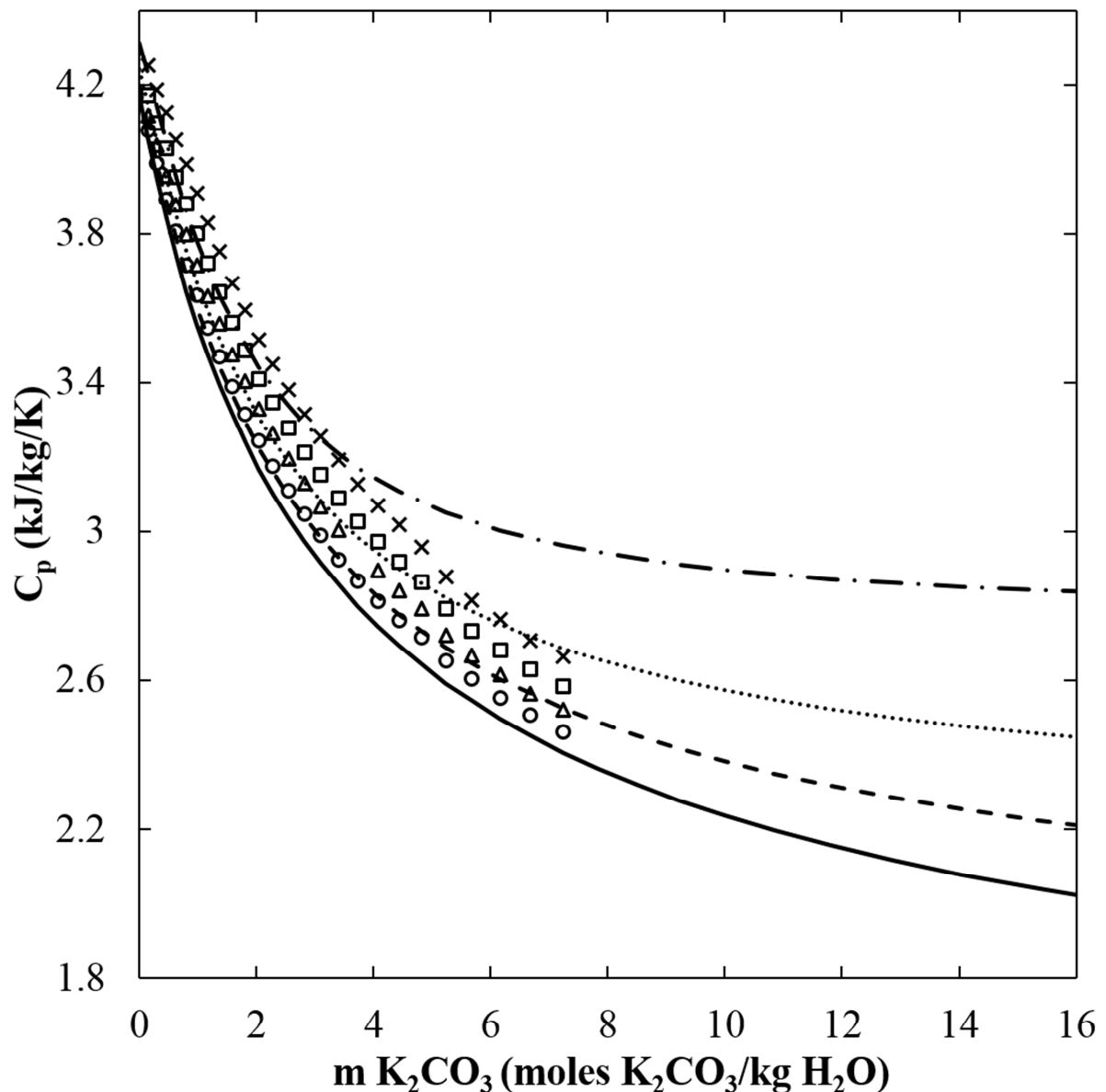


Figure 6. Heat capacity of aqueous K_2CO_3 solution with experimental data [30] in symbols and model results in lines at 323.15 K (\circ , —), 363.15 K (Δ , - - -), 393.15 K (\square ,), 423.15 K (\times , - · -)

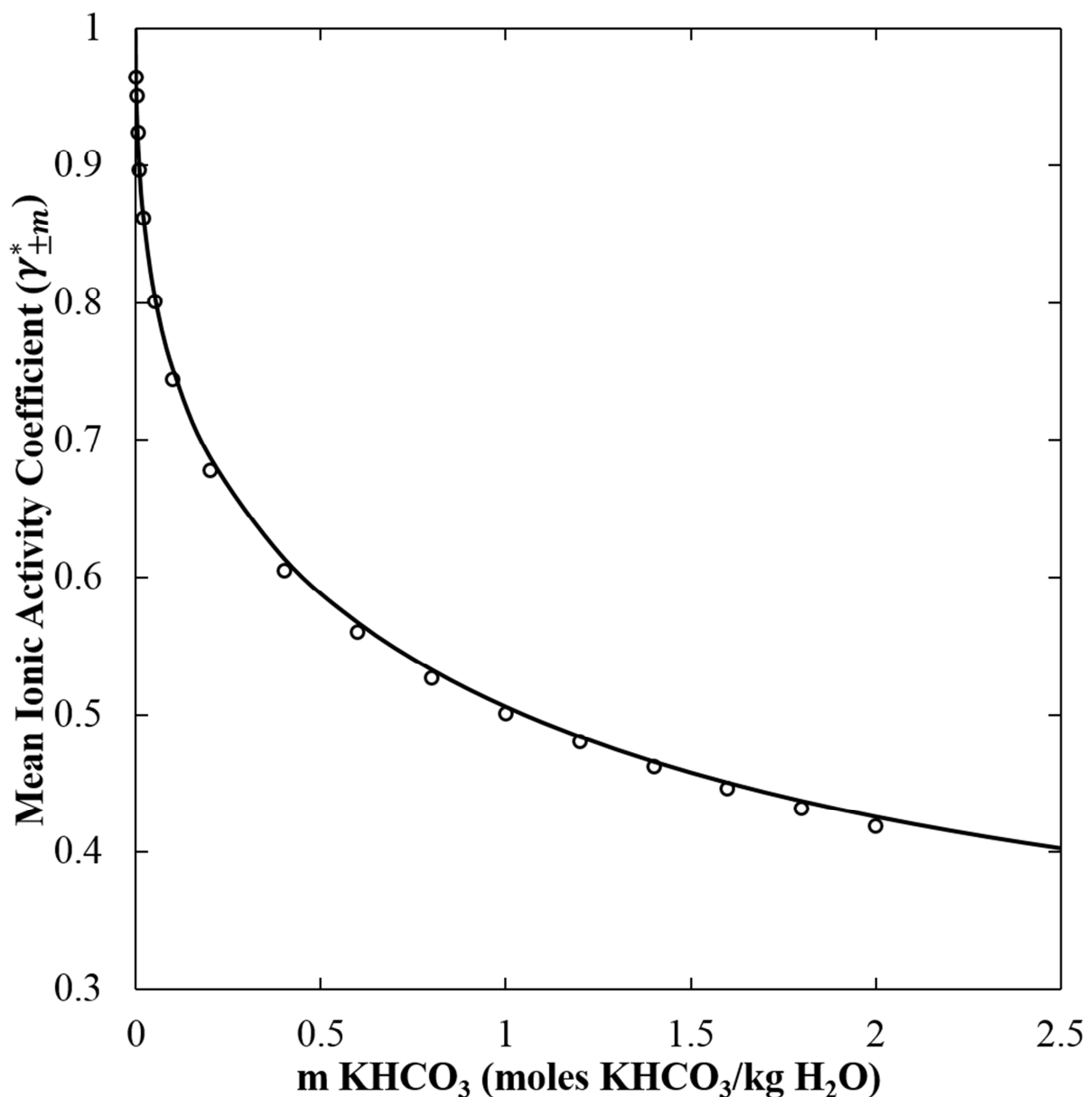


Figure 7. Molality-scale mean ionic activity coefficient of aqueous KHCO_3 solution with experimental data [31] (○) and model results (—) at 298.15 K

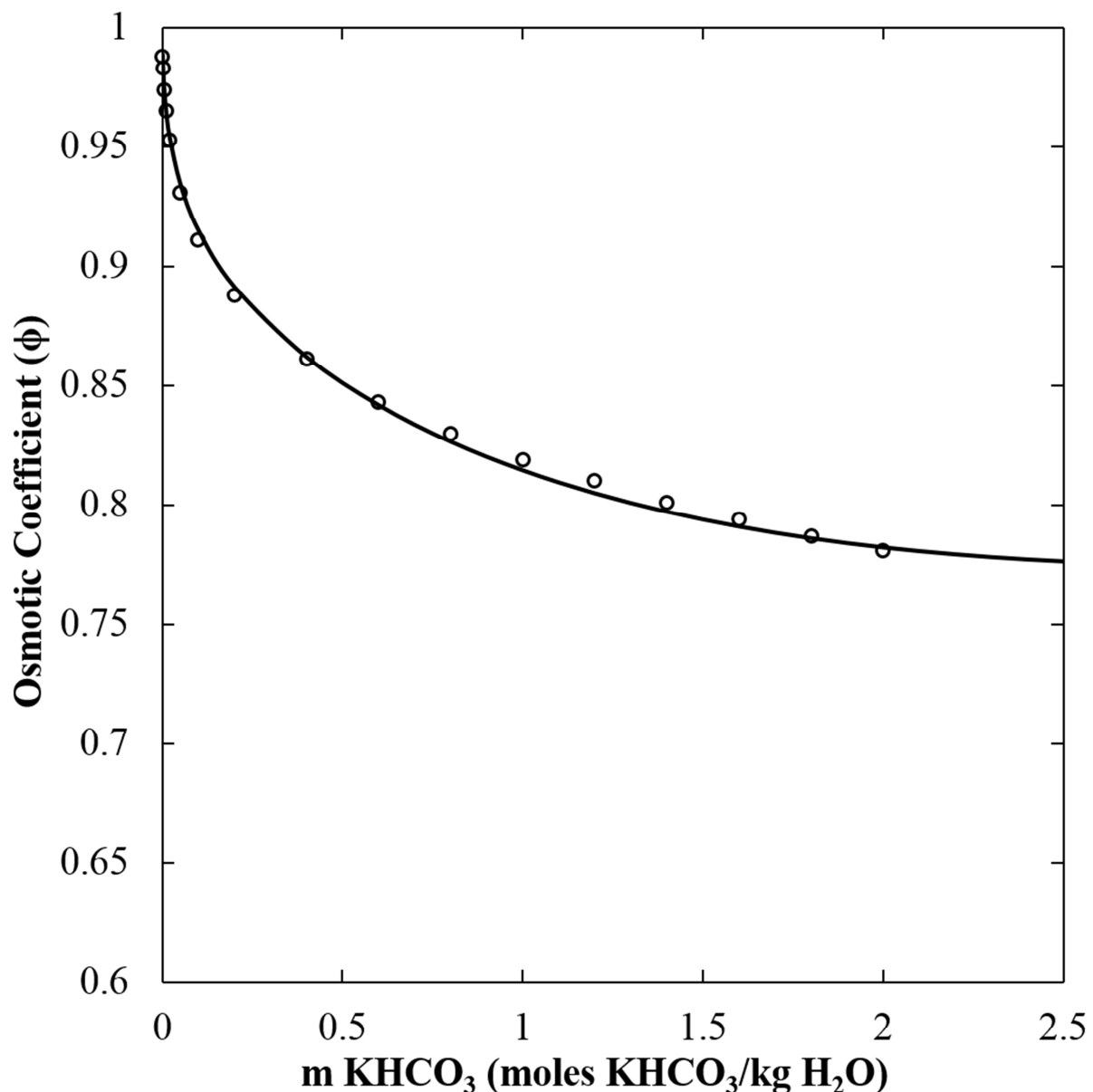


Figure 8. Osmotic coefficient of aqueous KHCO₃ solution with experimental data [31] (●) and model results (—) at 298.15 K

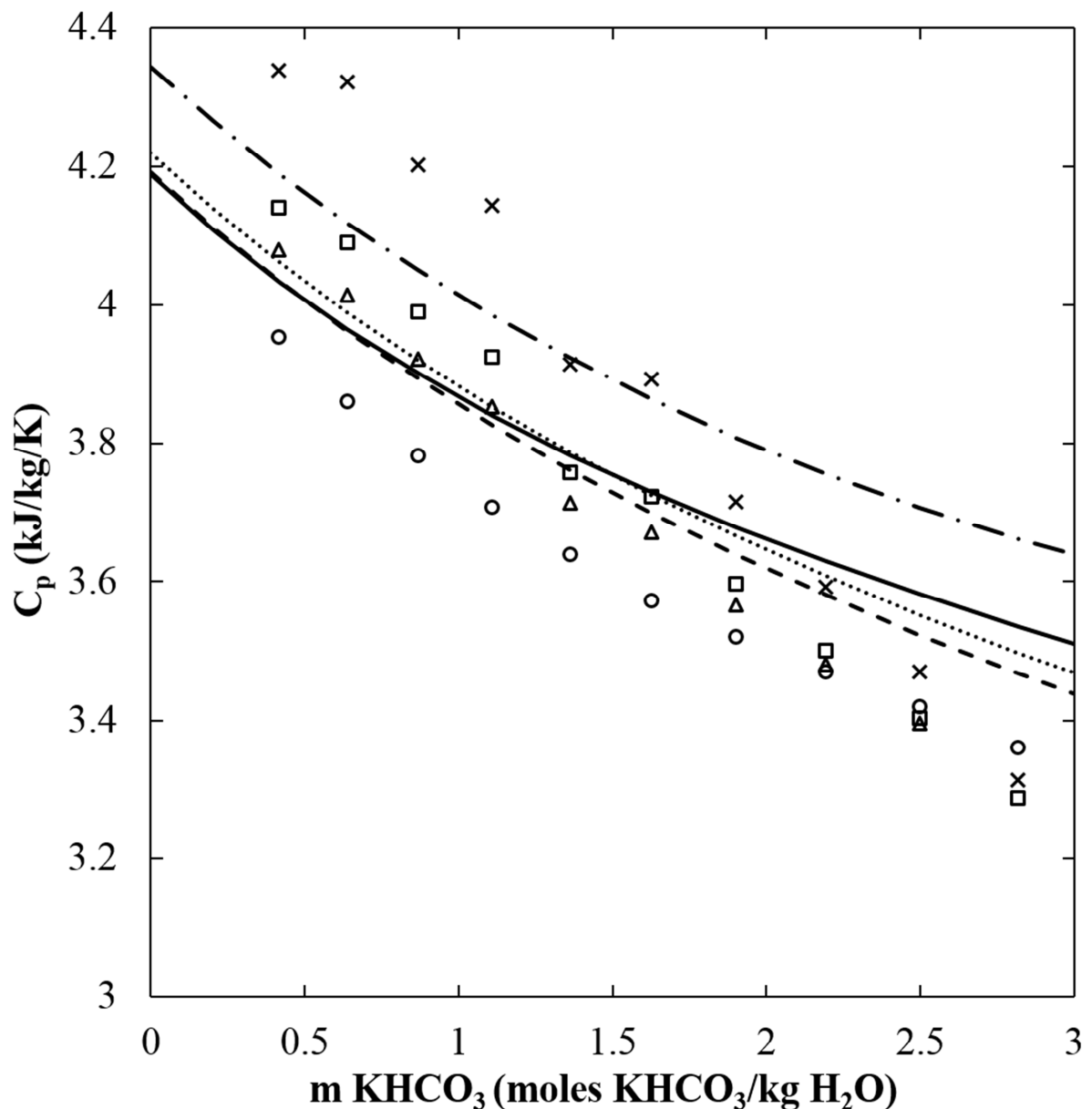


Figure 9. Heat capacity of aqueous KHCO_3 solution with experimental data [30] in symbols and model results in lines at 283.15 K ($\textcircled{\text{o}}$, —), 353.15 K (Δ , - - -), 378.15 K (\square ,), 433.15 K (\times , - · -)

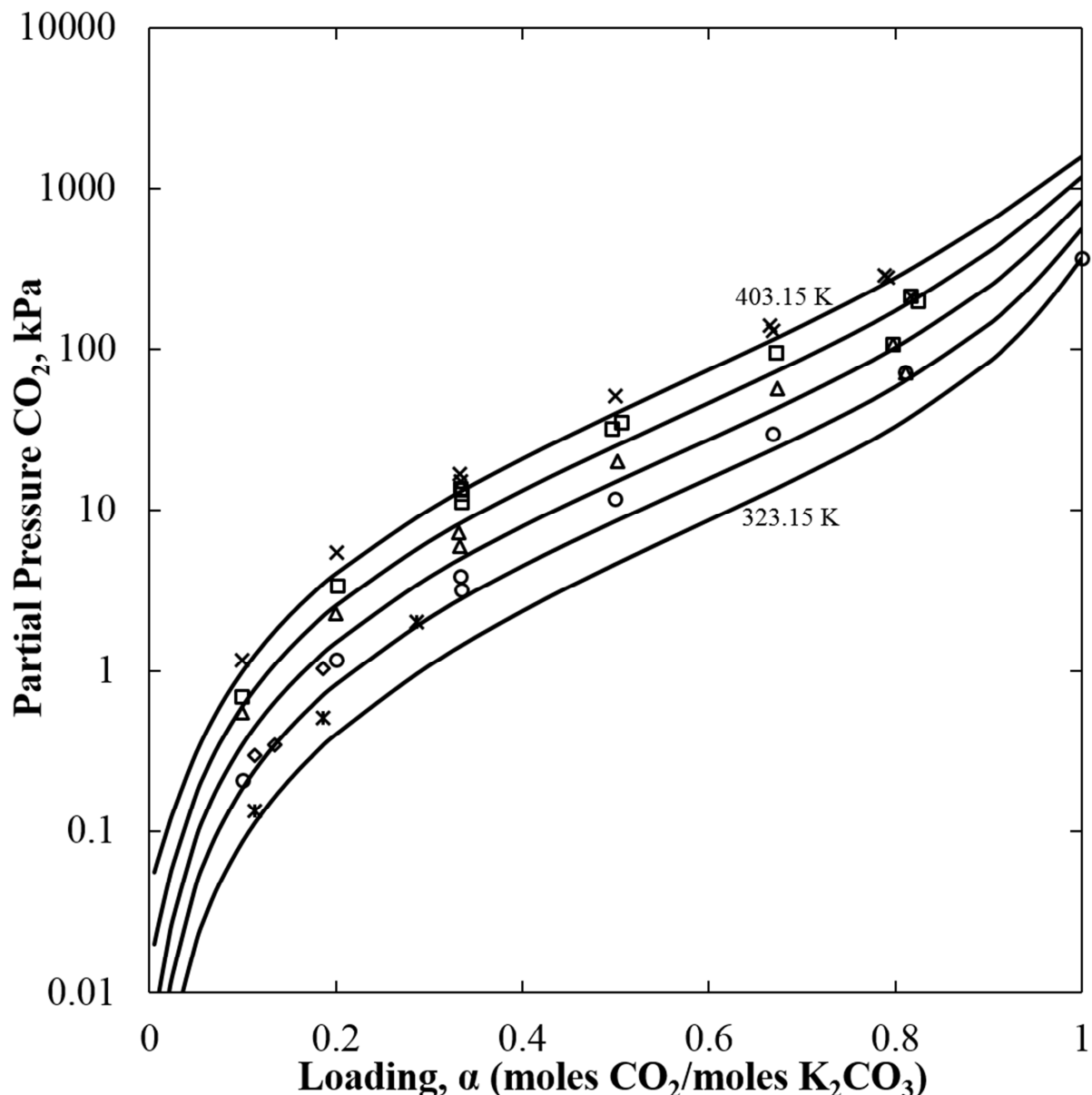


Figure 10. CO_2 partial pressure over 1.81 molal (20 wt.%) K_2CO_3 solution at different CO_2 loadings with experimental data in symbols and model results in lines (—) at 323.15 K ([34] *), 343.15 K ([8] O, [34] ♦), 363.15 K ([8] △), 383.15 K ([8] □), 403.15 K ([8] ×)

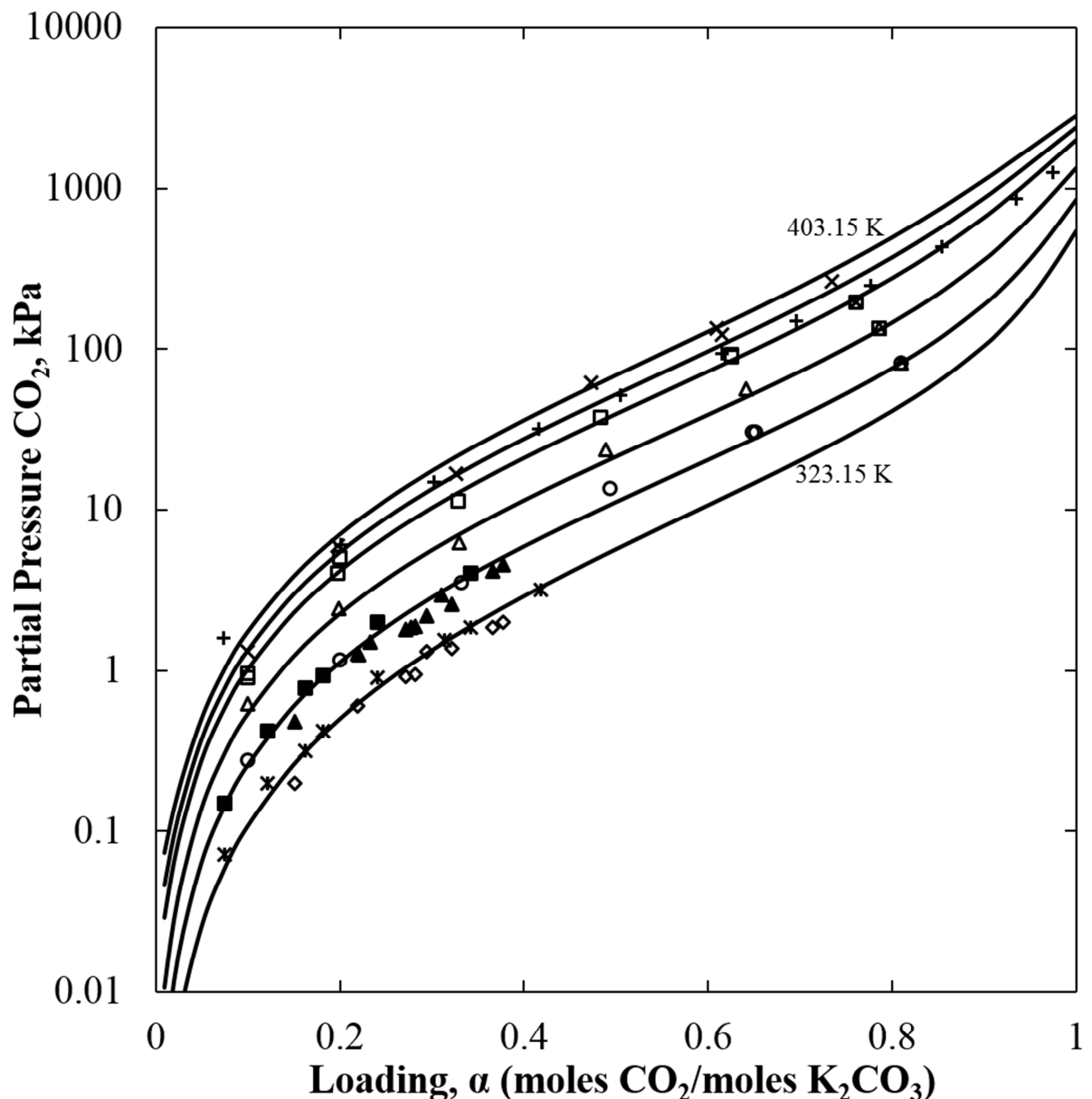


Figure 11. CO_2 partial pressure over 3.10 molal (30 wt.%) K_2CO_3 solution at different CO_2 loadings with experimental data in symbols and model results in lines (—) at 323.15 K ([4] \diamond , [34] $*$), 343.15 K ([4] \blacktriangle , [8] \bullet , [34] \square), 363.15 K ([8] Δ), 383.15 K ([8] \square), 393.15 K ([35] $+$), 403.15 K ([8] \times)

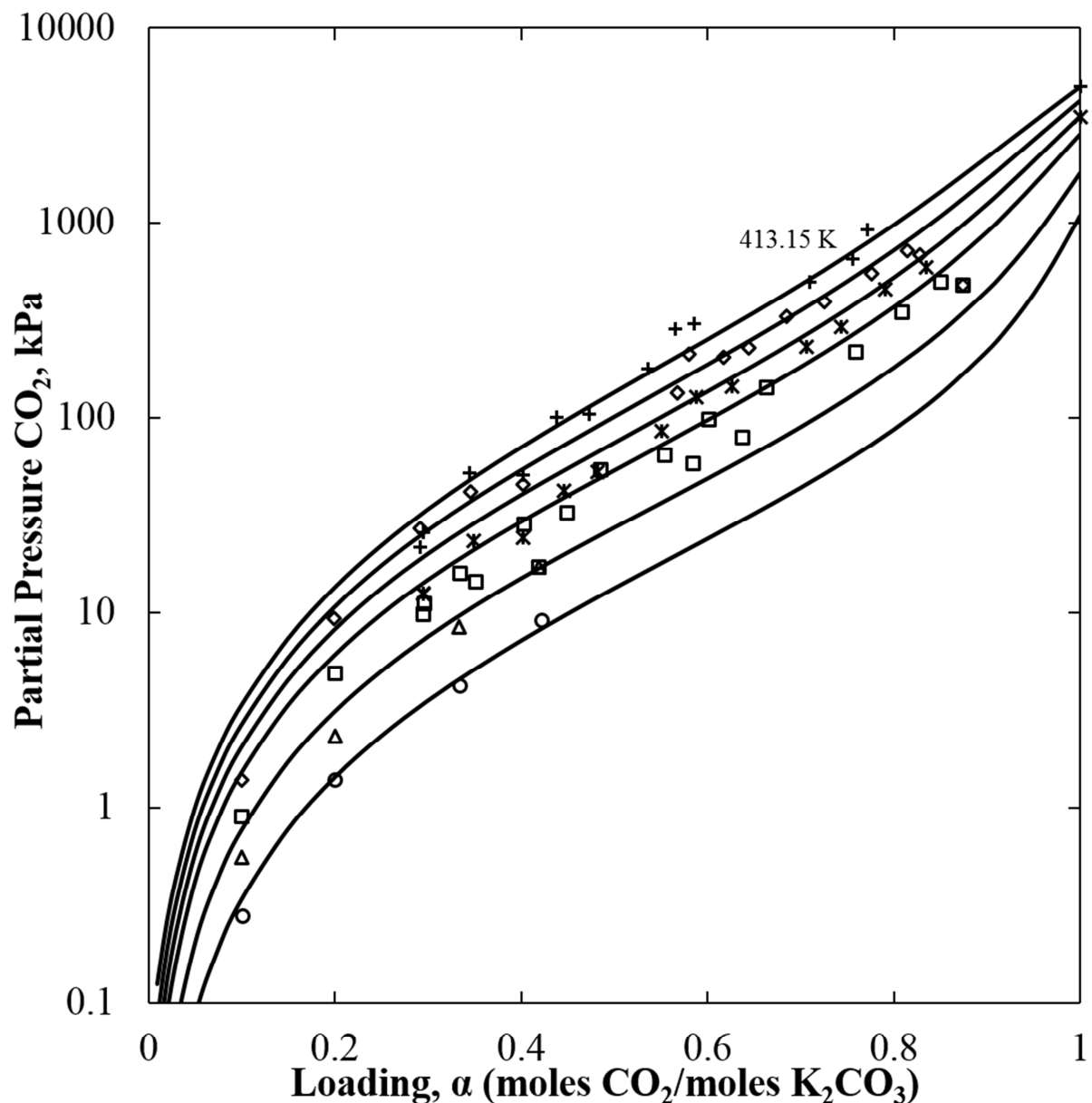
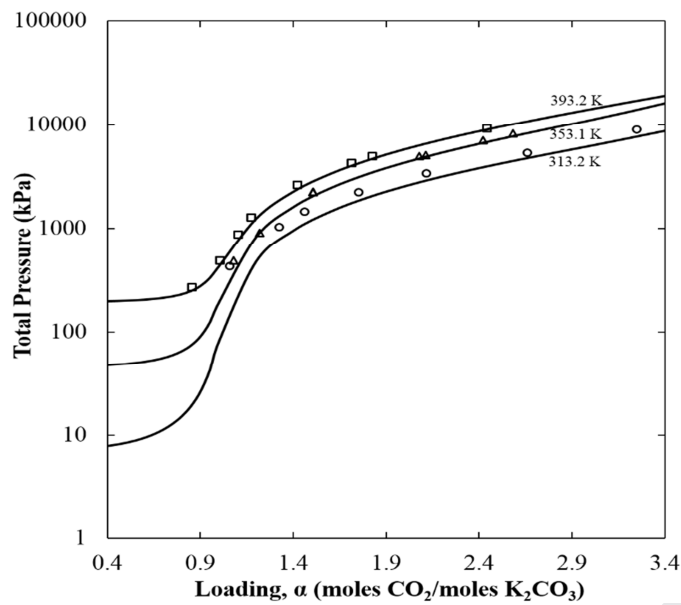


Figure 12. CO₂ partial pressure over 4.82 molal (40 wt.%) K₂CO₃ solution at different CO₂ loadings with experimental data [8] in symbols and model results in lines (—) at 343.15 K (○), 363.15 K (△), 383.15 K (□), 393.15 K (*), 403.15 K (◊), 413.15 K (+)

(a)



(b)

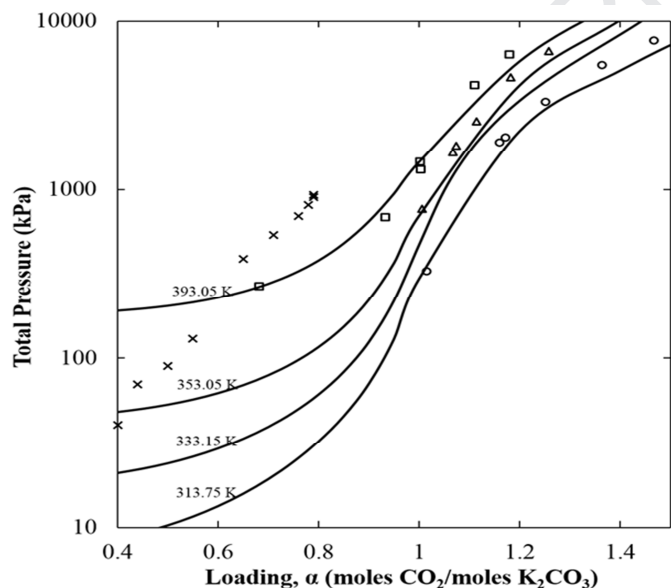


Figure 13. (a) Total pressure over low concentration K_2CO_3 solution at high CO_2 loading with experimental data in symbols [7] and model results in lines (—): 0.47 molal (\bullet) at 313.2 K, 0.43 molal (Δ) at 353.1 K and (\square) at 393.2 K. (b) Total pressure over high concentration K_2CO_3 solution at high CO_2 loading with experimental data in symbols and model results in lines (—): 1.71 molal [7] at 313.75 K (\bullet), 353.05 K (Δ), 393.05 K (\square) and 1.81 molal or 20 wt.% [16] at 333.15 K (\times)

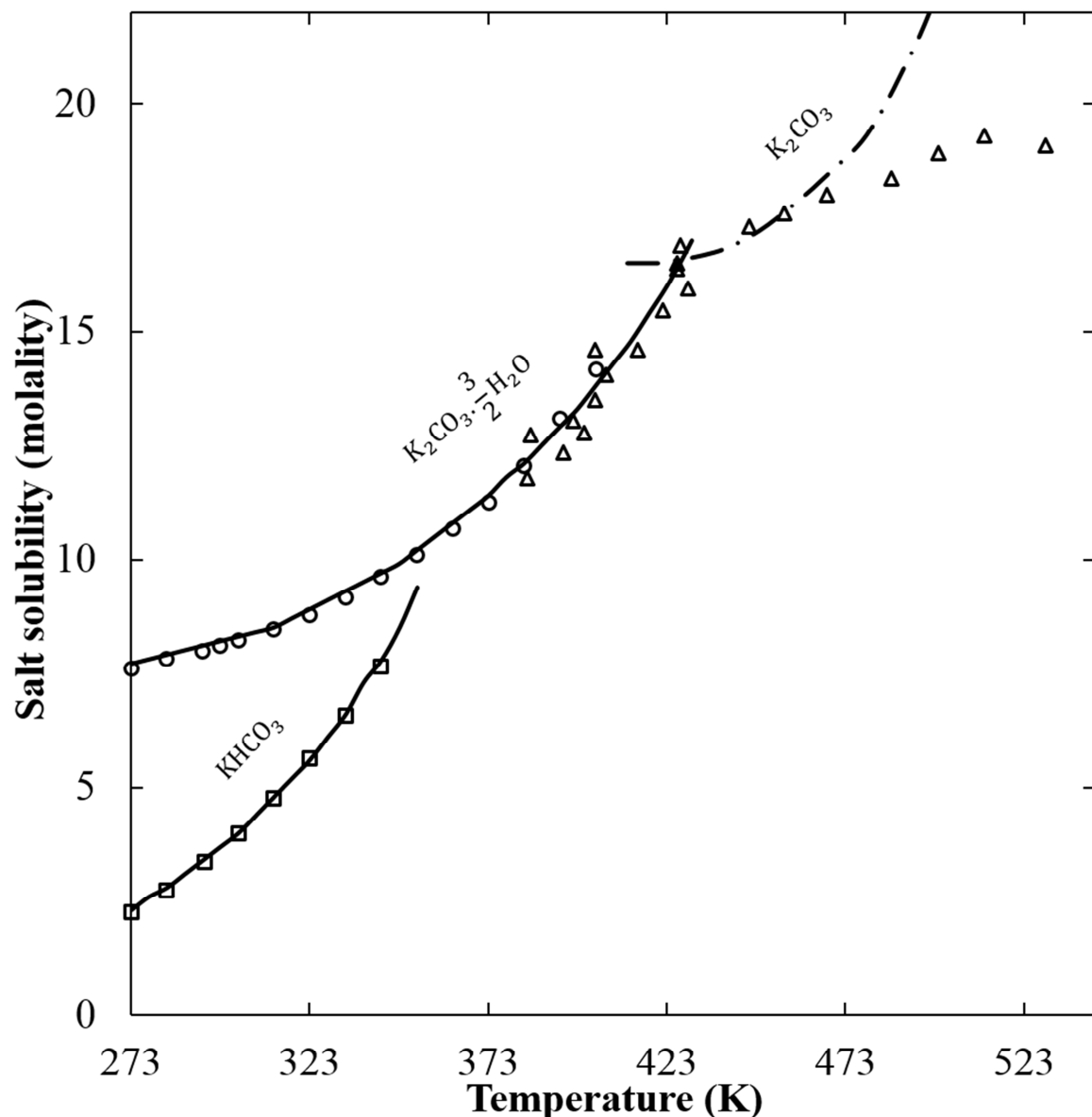


Figure 14. Salt solubility data [25] (○, □) [26] (△) for various salts in aqueous K_2CO_3 and KHCO_3 solutions vs. temperature with model results assuming (R7) chemistry (—), (R8) chemistry (---) and (R9) chemistry (— · —)